Research Article | Vol. 27, No. 3 | 4 Feb 2019 | OPTICS EXPRESS 2125
Optics EXPRESS

High-performance fully differential photodiode amplifier for miniature fiber-optic gyroscopes

SHAOBO ZHANG, CHUNXI ZHANG, XIONG PAN,* AND NINGFANG SONG

School of Instrumentation and Optoelectronic Engineering, Beihang University, Beijing 100191, China
**08768@buaa.edu.cn*

Abstract: Electrical cross coupling is regarded as a major obstacle to achieving high-performance miniature fiber-optic gyroscopes (FOGs), because it can cause dead bands, which are critical errors in FOGs. Using a differential photodiode amplifier has proven to be effective in rejecting coupled interference. However, the conventional three-op-amp instrumentation amplifier cannot provide a miniature FOG's bandwidth requirements, because of the large photodiode capacitance and parasitic capacitance. We present a high-performance, fully differential photodiode amplifier, where the bandwidth limitations are removed by applying a reverse bias to the photodiode and replacing the feedback resistor with a modified tee-network and a DC cancellation loop. For an experimental FOG with a 300 m fiber coil, we demonstrate a fully differential photodiode amplifier with 880 kΩ gain and 3.5 MHz bandwidth. In the FOG performance test, it not only reduces the angular random walk and bias drift, but also eliminates the approximately 1°/h dead band observed in the same FOG using a PINFET receiver, demonstrating its effectiveness in suppressing coupled interference.

1. Introduction

Fiber-optic gyroscopes (FOGs) of various grades have been used in several inertial rotation-sensing applications [1–3]. Currently, efforts are underway to achieve a high-performance FOG in a miniature design [3,4]. However, cross-coupling interference is one of the major obstacles to reaching this goal. In a closed-loop FOG, as illustrated schematically in Fig. 1, the electrical cross coupling between the modulation voltage and photodiode output current can cause a dead band, a range of rates where the FOG cannot sense, which degrades the FOG performance [5–10]. The modulation voltage is generally within the range of a few volts, while the primary photocurrent is typically few tens of microamperes [1]. With such high levels of amplitude differences on a common circuit board, it is impractical to remove the cross-coupling interference by isolation, shielding, or filtering, especially on a compact circuit board in a miniature FOG [11]. Two widely used modulation techniques, random modulation and dithering technique, have been proposed to suppress the dead band due to cross-coupling, but at the expense of increased random noise and reduced dynamic range [5]. On the other hand, increasing the common-mode rejection of the photodiode amplifier seems a more practical method because it can suppress not only the cross-coupling interference from the modulation voltage, but also any other common-mode interference or noise that may deteriorate the FOG performance. In addition, it can be used in combination with other modulation technique to provide a further suppression of the cross-coupling interference.

A typical photodiode amplifier consists of a photodiode that converts optical signal into current signal and an amplifier stage that converts current signal into voltage signal. The choice of photodiode is relatively straightforward, as it only depends on the wavelength and optical power used. For FOGs, semiconductor PIN photodiodes are ideal because of their very high quantum efficiency and the most commonly used materials are Si (for 850 nm) and InGaAs (for 1300 and 1550 nm) [1]. It is generally the amplifier stage that determines the

#348126 https://doi.org/10.1364/OE.27.002125
Journal © 2019 Received 16 Oct 2018; revised 13 Dec 2018; accepted 29 Dec 2018; published 24 Jan 2019

Optics EXPRESS

performance of a photodiode amplifier, including the noise, bandwidth, gain, and immunity to electromagnetic interference.

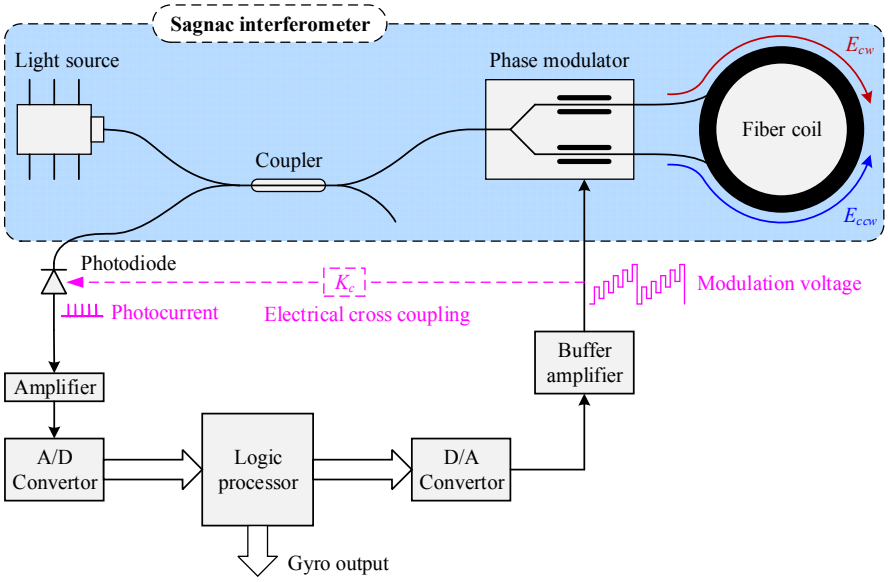

Fig. 1. Schematic of a closed-loop fiber optic gyroscope (FOG) showing the electrical cross-coupling path from the modulation voltage to the photodiode current. The FOG consists of a Sagnac interferometer (including a light source, coupler, phase modulator, and fiber coil) and electronic components (including a photodiode, preamplifier, analog/digital converter, logic processor, digital/analog converter, and buffer amplifier) mounted on a common circuit board.

Currently, technical literature on photodiode amplifier designs for FOGs is rather scarce. Much of the related studies address one of the two distinct domains: low-frequency (usually below 100 kHz) sensing applications requiring high sensitivity and low noise, or high-speed telecommunications receivers requiring wide bandwidths (usually in excess of 100 MHz) [12–14]. The FOG application typically lies between these two frequency extremes. As illustrated in Fig. 2, the current delivered by the photodiode consists of an AC signal carrying useful rotation rate information $\Delta\varphi_R$, an unwanted DC signal $I_0/2$, and undesirable current spikes generated periodically during each transition of phase modulation $\pm\varphi_m$. The amplitude of the AC signal corresponding to a rotation rate is usually very small (typically, 1 pA for an angular rate of l°/h); therefore, a low-noise, high-gain photodiode amplifier is necessary to maintain the FOG performance [1,15]. The frequency of the AC signal corresponding to the modulation frequency is strictly related to the length of the fiber, and typically ranges from 100 kHz (for 1000 m of fiber) to 1 MHz (for 100 m of fiber). To avoid the AC signal distortion due to saturation, clipping, or energy spread of the spikes, the gain of the photodiode amplifier must be chosen appropriately and the bandwidth of the photodiode amplifier must be sufficiently higher than the modulation frequency [15–17]. A rule of thumb is to provide a photodiode amplifier with a bandwidth that is an order of magnitude larger than the modulation frequency, i.e., ranging from 1 MHz to 10 MHz for FOG application [15]. At present, the most common type of photodiode amplifier used in FOGs is a PINFET hybrid receiver designed for telecommunications, which provides the required wide bandwidth, high gain, and low noise [1,18]. Other types of photodiode receivers have also been proposed, which mainly focus on intrinsic noise reduction and bandwidth improvement [15]. However, none of these designs focus on the rejection of coupled interference (from either the modulation voltage or the external electromagnetic signals), which may contribute more errors to a FOG than the intrinsic noise [12,19].

Optics EXPRESS

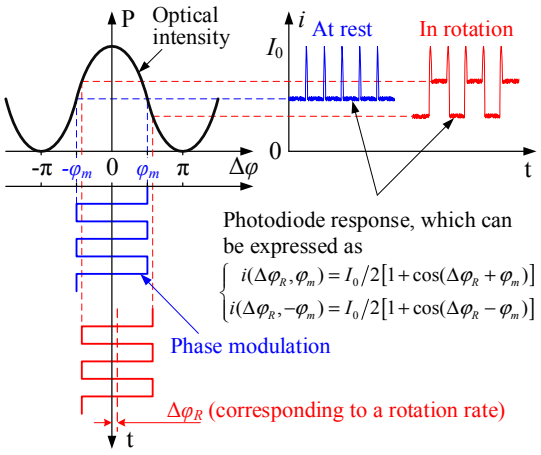

Fig. 2. Photodiode response to the applied phase modulation ± φ_m when the FOG is at rest or is subjected to rotation. $\Delta\varphi_R$ denotes the Sagnac phase caused by the rotation rate.

Using a differential photodiode amplifier has been proved to be an effective method to reject common-mode interfering signals [12]. The three-op-amp instrumentation amplifier topology (shown in Fig. 3(b)) and its simpler version (shown in Fig. 3(a)) are two of the available solutions for the differential configuration [20,21]. Although the simpler topology requires fewer components, the instrumentation amplifier topology is commonly preferred because it overcomes the bandwidth limitations of the simpler topology caused by the common-mode capacitance at the amplifier inputs. However, it still fails to meet the bandwidth requirements of a miniature FOG. The main limitations to the bandwidth of the instrumentation amplifier arise from the large photodiode capacitance at the amplifier inverting input and the parasitic capacitance across the large feedback resistor, as discussed in Section 2. Operating the photodiode in the photoconductive mode (with a reverse bias) can reduce the photodiode capacitance and using a resistive tee-network can reduce the effect of parasitic capacitance. However, they cannot be used simultaneously in the instrumentation amplifier, because an unacceptably large DC offset voltage will be produced at the circuit output, leading to output saturation in most cases.

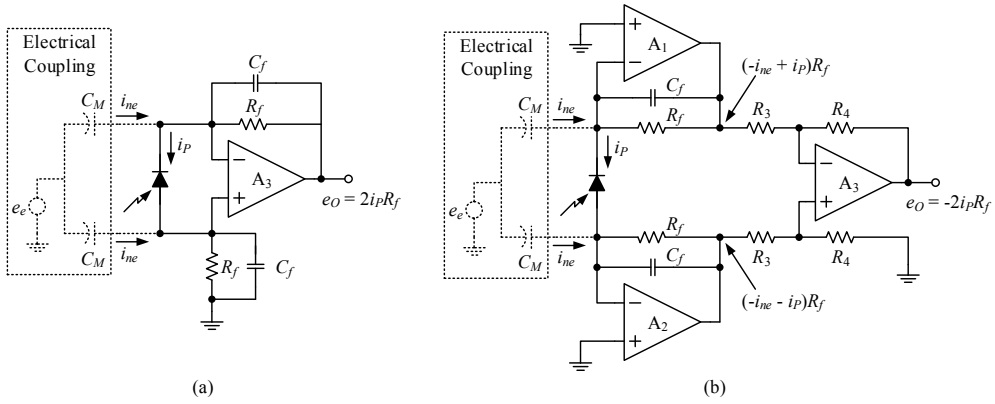

Fig. 3. Conventional differential photodiode amplifiers: (a) simpler topology, (b) three-op-amp instrumentation amplifier. Both of them are subjected to a common-mode interfering signal e_e and produce two equal noise currents i_{ne} that are then cancelled out by a differential amplifier.

To address this problem, this paper introduces an offset cancellation loop to the instrumentation amplifier, which consists of an integrator circuit intended to sense the DC

Optics EXPRESS

output offset and a modified tee-network intended to remove this offset automatically. In addition, the third amplifier of the three-op-amp instrumentation amplifier is replaced with a fully differential amplifier, offering the advantages of differential output, good common-mode rejection, and easy driving of the subsequent differential-input analog/digital converter (ADC). The choice of each component value is also studied in this paper to optimize the gain, bandwidth, and noise performance. Finally, a fully differential photodiode amplifier with a gain of 880 kΩ and bandwidth of 3.5 MHz is demonstrated for a 300 m FOG. To the best of our knowledge, this is the first fully differential photodiode amplifier suited for FOGs, which provides the required wide bandwidth, high gain, and low noise. The most important advantage is that it exhibits good rejection of coupled interference, resulting in a significant improvement in the FOG performance. The experimental results show that the fully differential photodiode amplifier improves the angle random walk (ARW) from 0.015 to $0.014\,°/\sqrt{\text{h}}$, reduces the bias drift from 0.12 to 0.03°/h, and eliminates the approximately 1°/h dead band.

The next section starts with description of the bandwidth limitations of the three-op-amp instrumentation amplifier. The proposed solution to these limitations, i.e., a modified differential photodiode amplifier with DC cancellation loop, is described in Section 3, along with its design details and noise performance analysis. Section 4 describes the experimental results with a prototype designed for a 300 m FOG, and Section 5 concludes this paper.

2. Bandwidth limitations of the three-op-amp instrumentation amplifier

2.1 Bandwidth limitation due to photodiode capacitance

The three-op-amp instrumentation amplifier can be easily understood by considering it as a pair of classic transimpedance amplifiers (TIAs) followed by a differential amplifier [12]. It has an almost similar performance as the classic TIA, except for its doubled transimpedance gain. Figure 4(a) shows the circuit model for bandwidth analysis [21,22]. In this model, the photodiode acts as a current source i_P with a junction capacitance C_D and shunt resistance R_{SH}. R_{SH} is generally ignored because its high value has little effect on the circuit. On the contrary, C_D has profound performance effects on the stability, bandwidth, and noise.

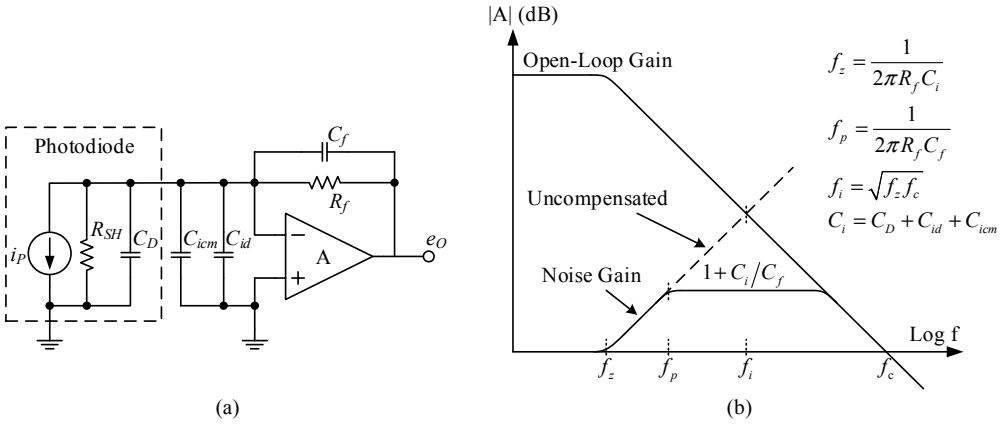

Fig. 4. (a) Circuit model and (b) noise-gain plot of a classic transimpedance amplifier (TIA) for the bandwidth analysis of the three-op-amp instrumentation amplifier.

As illustrated in the Bode plot of Fig. 4(b), C_D, along with the amplifier's differential-mode input capacitance C_{id} and common-mode input capacitance C_{icm}, produces a response zero in the reciprocal of the feedback factor $1/\beta$ (or the noise gain) at the frequency of $f_z = 1/2\pi R_f C_i$, where $C_i = C_D + C_{id} + C_{icm}$ denotes the total input capacitance. If left

Optics EXPRESS

uncompensated, the $1/\beta$ curve will rise and intercept the amplifier open-loop gain A_{OL} at the frequency of $f_i = \sqrt{f_z f_c}$ (shown by the dashed line), where f_c is the unity-gain bandwidth frequency of the amplifier. The rate of closure between the two curves is 40 dB/decade, corresponding to 180° of phase shift, which can cause instability and oscillations. Adding a phase-compensation capacitor C_f across the feedback resistor R_f can stabilize the circuit by introducing a pole at $f_p = 1/2\pi R_f C_f$, which levels the noise gain at $1 + C_i/C_f$. Note that f_p is also the signal bandwidth, which must satisfy the condition $f_p \le f_i$. Therefore, for a given gain, the best bandwidth is f_i, which can be obtained when the capacitor

$$C_f = \sqrt{\frac{C_i}{2\pi R_f f_c}}. \tag{1}$$

Further improvement of the signal bandwidth needs further reduction in C_f. There are two ways to achieve this: by decreasing C_i or by increasing f_c. Increasing f_c is beneficial for the bandwidth, but it also increases the output noise. In contrast, decreasing C_i is beneficial for both the bandwidth and noise because it moves the response zero f_z to a higher frequency and lowers the noise-gain plateau. This can be achieved by selecting an amplifier with low input capacitances and reverse biasing the photodiode to reduce the junction capacitance C_D. As the total input capacitance C_i is always dominated by the photodiode capacitance C_D, reverse biasing the photodiode is a simple but effective way to improve the bandwidth, and thus is widely used in high-speed applications [23].

2.2 Bandwidth limitation due to parasitic capacitance

Even if all the above-mentioned methods were adopted, the signal bandwidth may still be poor because the high value of R_f reduces the value of C_f to such a low level that the parasitic capacitances significantly alter the desired bandwidth [24]. For example, for a desired bandwidth of approximately 5 MHz with a feedback resistor of 100 kΩ, a feedback capacitor of 0.3 pF is required. However, the parasitic capacitance across the feedback path will probably be in the order of 1 pF to 2 pF, limiting the bandwidth to approximately 1 MHz. A resistive tee-network can overcome such a problem by introducing a voltage divider of R_1/R_2 to the feedback loop, as illustrated in Fig. 5 [21]. For an equivalent gain, the value of the feedback resistor can be decreased by a factor of 1 + R_1/R_2, i.e., $R_{feq} \approx (1 + R_1/R_2)R_{fT}$ (for $R_{fT} >> R_1$). Thus, for an equivalent bandwidth, the value of C_f can be increased by the same factor, reducing its sensitivity to parasitic capacitances. In addition, the parasitic capacitance across the feedback path is also reduced because of the added physical spacing of the tee-network with three resistors instead of one.

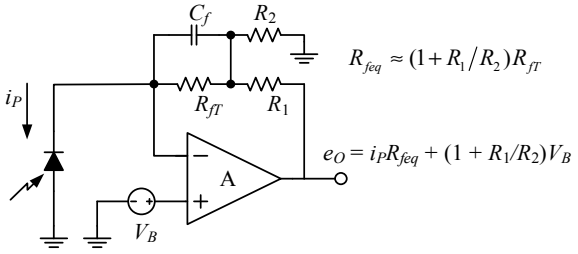

Fig. 5. Tee-network intended to reduce the effect of parasitic capacitances. The bias voltage V_B at the non-inverting input is also amplified by the tee-network to produce a large output offset.

However, the tee-network also amplifies the bias voltage V_B at the non-inverting input by the same factor, to produce a large output offset voltage, $(1 + R_1/R_2)V_B$. Therefore, when

Optics EXPRESS

combining the tee-network with an instrumentation amplifier operated in the photoconductive mode (whose reverse bias can only be applied at the non-inverting input), the DC offset voltage at the circuit output will be increased to an unacceptably high value, leading to output saturation in most cases.

3. Modified differential photodiode amplifier with DC cancellation loop

3.1 Circuit analysis

To address the saturation problem, we modified the tee-network and introduced a DC cancellation loop to the three-op-amp differential amplifier. As illustrated in the modified TIA in Fig. 6, the third node of the tee-network was connected to a DC voltage V_T rather than to the ground. This DC voltage V_T also produced a large output offset voltage that could be used to counteract the output offset caused by the bias voltage V_B. This effect can be described as

$$e_O = i_P(1+R_1/R_2)R_{fT} + \underbrace{(1+R_1/R_2)V_B - (R_1/R_2)V_T}_{\text{DC offset}}. \tag{2}$$

C_f is neglected here and in the following DC offset analyses. As can be seen, the DC offset can be eliminated if $V_T = (1+R_2/R_1)V_B$. While adding a corresponding DC voltage is a solution, using an integrator circuit to sense the total output offset and using its output to supply V_T is a better approach. Therefore, the modified tee-network and integrator circuit comprised an offset-reduction feedback loop that automatically compensated for the DC output offset. In the steady state, the voltage V_T was maintained at a fixed value, which could just counteract the DC component in the circuit output.

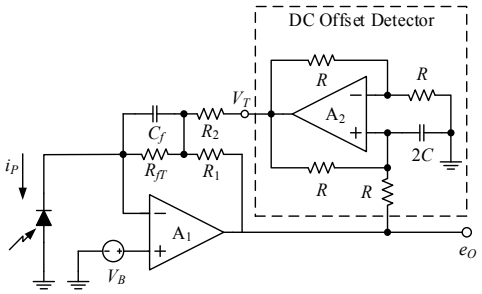

Fig. 6. Basic structure of the modified TIA with a DC cancellation loop.

To achieve negative feedback, the sign of V_T (output of the integrator circuit) should be the same as that of the output offset (input of the integrator circuit); therefore, a Deboo integrator (within the dashed box in Fig. 6) was adopted here to achieve non-inverting integration [25]. Its transfer function is given by

$$H(s) = \frac{1}{RCs}, \tag{3}$$

which is the same as that of the popular Miller integrator, except for the opposite sign. Substituting it into Eq. (2) yields:

$$e_O = (1+A)(i_P R_{fT} + V_B) - \frac{A}{RCs}e_O, \tag{4}$$

where $A = R_1/R_2$. Further, the output of the modified TIA is expressed as

Optics EXPRESS

$$e_O = (1+A)(i_P R_{fT} + V_B)\frac{RCs}{A+RCs}. \quad (5)$$

Compared to the output of the tee-network expressed in Fig. 5, the offset-reduction loop added an element with high-pass transfer characteristics to Eq. (5), thereby eliminating the low-frequency components of the output. This offset-reduction loop behaved like an attached AC-coupling capacitor, with the difference that it removed the DC output offset in the input stage. A particular advantage of this approach was that the gain limit imposed by the unwanted DC current generated in the photodiode was removed, indicating that the maximum transimpedance gain could be doubled to improve the signal-to-noise ratio (SNR) [26].

The complete circuit schematic of the modified differential amplifier is shown in Fig. 7. One slight modification to the Deboo integrator is the shifting of half of the capacitance $2C$ to the negative feedback path, without changing the transfer function, which can reduce the noise contribution of the integrator, as described below. Another modification to the three-op-amp instrumentation amplifier is the replacement of the differential-to-single-ended amplifier with a fully differential amplifier, which offers the advantages of differential output, better common-mode rejection, and easy driving of the subsequent differential input ADC. To further improve the common-mode rejection, the differential signal path should be matched tightly. In addition to the careful circuit layout, the values of the resistors and capacitors should be chosen carefully to obtain small component tolerance and avoid parasitic effects.

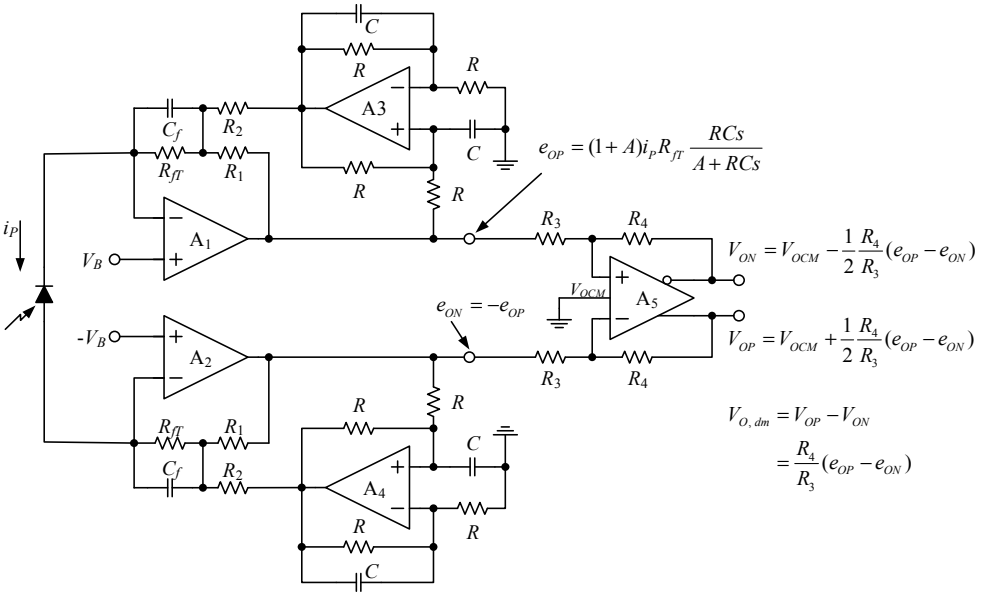

Fig. 7. Complete circuit schematic of the proposed fully differential photodiode amplifier, consisting of two matching modified TIAs shown in Fig. 6 and a fully differential amplifier A_5.

3.2 Signal bandwidth and gain

The complete transfer function of the differential amplifier including C_f can be obtained by replacing the R_{fT} element in Fig. 7 with $R_{fT} \parallel (1/sC_f)$, which can then be expressed as

$$\frac{V_{O,dm}}{i_P} = 2\frac{R_4}{R_3}\frac{(1+A)R_{fT}}{1+R_{fT}C_f s}\frac{RCs/A}{1+RCs/A}, \quad (6)$$

Optics EXPRESS

giving a band-pass response with a zero at the origin and two real poles at $-1/R_{fT}C_f$ and $-A/RC$. Accordingly, the lower and upper −3 dB cut-off frequencies are given by $f_L = A/2\pi RC$ and $f_H = 1/2\pi R_{fT}C_f$, respectively. The signal bandwidth is described as $f_H - f_L$ and should be centered at the modulation frequency f_{mod}. The overall gain in the passband is the product of the first- and second-stage gains, $2(1+A)R_{fT}$ and R_4/R_3. To improve the SNR, it is desirable to maximize the first-stage gain, without risking saturation or clipping.

A number of design compromises must be made when determining the signal bandwidth and gain. As stated above, the frequency spectrum of the photocurrent signal is quite broad; therefore, both f_L and f_H must be sufficiently far apart from f_{mod} to avoid signal distortion. In general, satisfying the condition $10f_L \le f_{\text{mod}} \le 0.1f_H$ is sufficient. f_L can be lowered in a straight-forward manner by choosing a large value for the RC time constant. However, this will cause the feedback loop to take a long time to settle to the final state and worsen the matching condition between the differential signal paths. Similarly, the values of R_{fT} and C_f should be chosen carefully to acquire a high transimpedance gain, high value of f_H, and good matching condition. Owing to the amplifying factor of (1 + A) provided by the tee-network, an intermediate value of R_{fT} (typically tens of kilo-ohms) would be a good compromise solution. The value of C_f should be as small as possible to enlarge f_H, but not smaller than the value in Eq. (1) to ensure circuit stability.

In our design of the differential photodiode amplifier for a nominal 300 m FOG, corresponding to a modulation frequency of approximately f_{mod} = 333 kHz, the required signal bandwidth was approximately between f_L = 30 kHz and f_H = 3 MHz, with a target first-stage transimpedance of approximately 400 kΩ (determined by the light source selected). According to the datasheet of the chosen PIN photodiode, the junction capacitance C_D was typically 7 pF and approximately 2 pF for 5 V reverse bias, which was the case in our design (i.e., V_B = 2.5 V). The input-stage amplifiers selected, A_1 and A_2, were a pair of FET input op-amps ADA4817, providing low input capacitance (C_{id} = 0.1 pF and C_{icm} = 1.3 pF typically), wide unity-gain bandwidth ($f_c \ge$ 410 MHz), and ultralow noise (4 nV/$\sqrt{\text{Hz}}$, 2.5 fA/$\sqrt{\text{Hz}}$). In this case, it was safe to assume that the total input capacitance C_i = 4 pF. For a given gain, $2(1 + A)R_{fT}$ ≈400 kΩ, the trade-offs among bandwidth, stability, noise gain, and matching condition determined the value of each resistor of the tee-network to be R_{fT} = 20 kΩ, R_1 = 100 Ω, and R_2 = 10 Ω. According to Eq. (1), the minimum value of C_f required to stabilize the circuit was 0.3 pF. On the other hand, the maximum value of C_f required to meet the bandwidth requirement was 2.6 pF. Considering the potential parasitic capacitance across each resistor, it was safe to use a phase-compensation capacitor of C_f = 1 pF. The integrator circuits were built with a dual op-amp AD8066, resistors of R = 10 kΩ, and capacitors of C = 0.1 μF, resulting in an ideal bandwidth from f_L ≈1.6 kHz to f_H ≈8 MHz. The fully differential amplifier circuit was built with AD8139, R_3 = 510 Ω, and R_4 = 1 kΩ, providing a second-stage gain of 2. All these op-amps were powered by ± 5 V supplies. When driving a differential-input ADC, the V_{OCM} pin of AD8139 should be supplied by the voltage reference pin of the ADC. In addition, an anti-aliasing filter should be added in front of the ADC to attenuate high-frequency noise. According to these parameters, the transfer function of the differential amplifier was simulated using SPICE, and further compared with that of the three-op-amp instrumentation amplifier, as shown in Fig. 8. The simulation parameters were listed and both of the feedback capacitors C_f were set to 1 pF, because the parasitic capacitance across the feedback path is generally in the order of 1 pF to 2 pF. For a given transimpedance gain of 118 dBΩ (880 kΩ), the bandwidth of the three-op-amp instrumentation amplifier was limited to 740 kHz, whereas the differential amplifier's bandwidth was improved to 8 MHz.

Optics EXPRESS

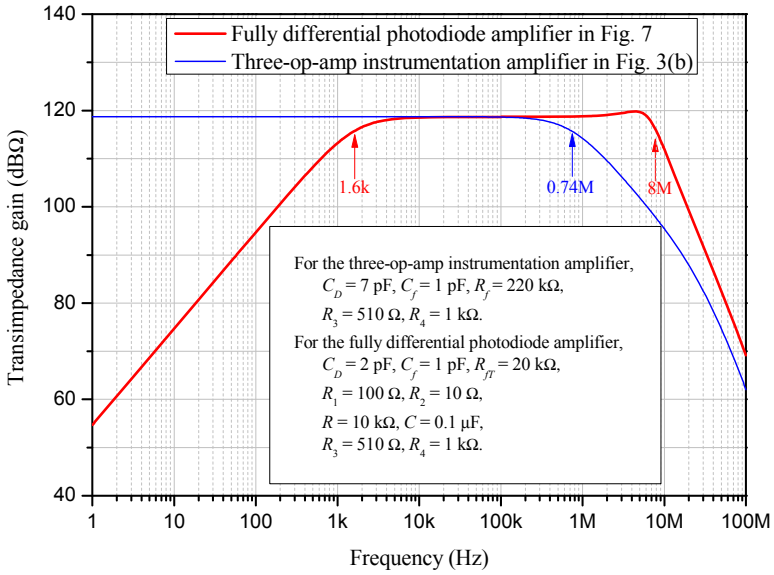

Fig. 8. SPICE simulated transfer functions of the fully differential photodiode amplifier and three-op-amp instrumentation amplifier, along with the simulation parameters used.

3.3 Noise performance

Although coupled interference can always dominate the output noise in practice, the circuit's inherent noise needs to be analyzed for a generalized application environment. There are five primary sources of noise in any photodiode amplifier system: shot noise, photodiode Johnson noise, amplifier current noise, feedback Johnson noise, and amplifier voltage noise [12,21]. The first two terms are related to the photodiode and both will be amplified by the signal gain along with the useful current signal. For this reason, shot noise and photodiode Johnson noise are not considered in the noise analysis of the proposed photodiode amplifier, in this paper. To simplify the analysis, the approach used in the three-op-amp instrumentation amplifier can be followed [21]. The noise effect of the second stage (including the fully differential amplifier A_5 and resistors R_3 and R_4) is negligible, because it enters the signal path after the high gain provided by the first stage. The noise analysis of the first stage is simplified by splitting it into two matching halves, i.e., two identical circuits as shown in Fig. 6, and introducing a $\sqrt{2}$ multiplier and the second-stage gain R_4/R_3 to the noise effect of either half to achieve the final result. The noise equivalent model with all noise sources is shown in Fig. 9(a), where a voltage noise generator e_{nINT} represents the noise effect of the integrator circuit.

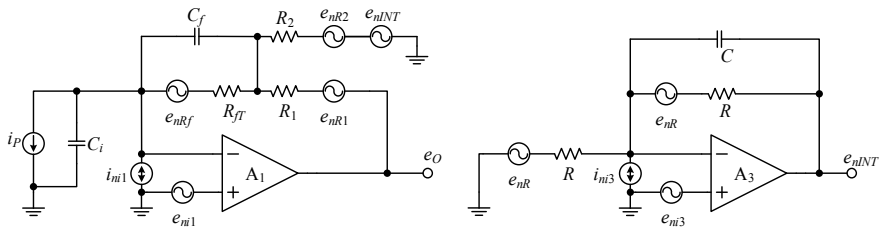

Fig. 9. (a) Noise equivalent model for the modified TIA in Fig. 6, where e_{nINT} denotes the noise effect of the Deboo integrator; (b) noise equivalent model for the Deboo integrator.

Optics EXPRESS

The amplifier current noise i_{ni1} represents the shot noise of the input bias current of the amplifier and can be neglected here because of the use of the low-bias-current FET input amplifier ADA4817. The Johnson noise of a resistor R has a spectral density of $e_{nR} = \sqrt{4kTR}$, where k = 1.38 × 10^{-23} J/K is Boltzmann's constant and T is the absolute temperature in Kelvin. Unlike the classic TIA, whose feedback Johnson noise appears directly at the output, each resistor of the tee-network contributes an amplified Johnson noise to the output: $(1+A)\sqrt{4kTR_{fT}}$ for R_{fT}, $A\sqrt{4kTR_2}$ for R_2, and $\sqrt{4kTR_1}$ for R_1. The first term may dominate the total output noise because of the added gain (1 + A), whereas the latter two terms can be neglected because of their small resistance values compared to R_{fT}. The integrator's noise e_{nINT}, in the same path as R_2, will be transferred to the output with the same amplification A. If left unfiltered, e_{nINT} will contribute significant noise as well.

The noise equivalent model for the Deboo integrator can be simplified to a simple non-inverting amplifier, as shown in Fig. 9(b), because the large capacitor C at the non-inverting input will bypass most of the noise to the ground, including the Johnson noise of the two resistors R and the noise contained in the input signal (i.e., the output signal e_O of amplifier A_1). The amplifier current noise i_{ni3} can also be neglected because of the use of the FET input amplifier AD8066. However, without the feedback capacitor C, the Johnson noise of the two resistors at the inverting input will appear directly at the output e_{nINT}, the amplifier voltage noise e_{ni3} will be transferred to the output e_{nINT} with the circuit's noise gain, 1 + R/R = 2, and both of these will contribute to the total output noise with amplification A. This problem can be solved by adding a large feedback capacitor C, which significantly reduces the noise bandwidth and makes e_{nINT} negligible. It is to be noted that while the added feedback capacitor will alter the transfer function of the Deboo integrator, taking half of the capacitance at the non-inverting input as the feedback capacitor (see Figs. 6 and 7) will keep it unchanged.

Referring back to Fig. 9(a), the amplifier voltage noise e_{ni1} makes the most complex and often the most significant contribution to the total output noise, as a result of the noise gain peaking (as illustrated in Fig. 4) caused by the input capacitance C_i. The noise gain of the tee-network in Fig. 9(a) can be expressed as [21]:

$$A_{\text{neT}} \approx (1+A)\frac{1+R_{fT}(C_i+C_f)s}{1+R_{fT}C_f s}. \tag{7}$$

Compared to the noise-gain curve of the classic TIA in Fig. 4, the tee-network adds an amplifying factor of (1 + A) to the noise-gain expression. However, for an equivalent signal gain and bandwidth, this amplifying factor may be ineffective at some frequencies. This inference is confirmed by the SPICE simulated noise-gain curves in Fig. 10(a), in which the parameters used in the simulations are listed. As the values of R_{fT} and C_i are decreased and the value of C_f is increased in the modified TIA, the response zero $1/2\pi R_{fT}(C_i+C_f)$ moves to a higher frequency (from ~100 kHz to ~1 MHz) and the gain plateau $1+C_i/C_f$ is reduced to a lower level (from 82 to 38), resulting in greatly reduced noise gain at higher frequencies (above 1 MHz). In addition, the integrator circuit introduces a response pole at ~1.6 kHz, lowering the noise gain at the lower frequencies as well. The amplified noise gain lies only in the small frequency range from ~100 Hz to ~1 MHz, which contributes negligible noise to the output because of the amplifier's low voltage noise (which is typically 4 nV/$\sqrt{\text{Hz}}$) and relatively small noise gain of 11.

Optics EXPRESS

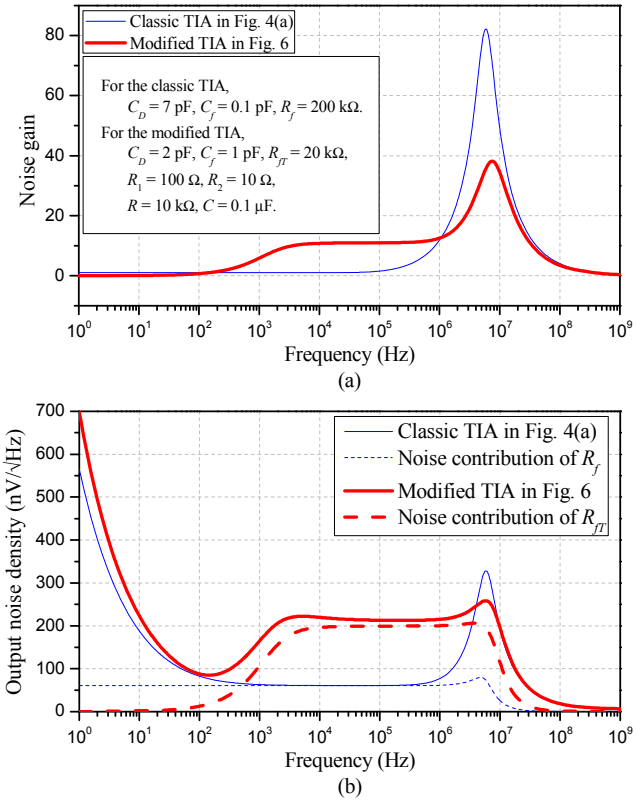

Fig. 10. SPICE simulated (a) noise gains and (b) output noise densities of the classic TIA in Fig. 4(a) and the modified TIA in Fig. 6. The simulation parameters are listed in Fig. 10(a).

The output noise densities created by the above noise contributors were simulated using the same SPICE models and parameters, with the contribution of the feedback Johnson noise presented separately, as shown in Fig. 10(b). Note that the simulated result of the modified TIA is related to the first-stage output e_{OP} in Fig. 7, for comparison with the classic TIA, and the approximate noise density of the differential output $V_{O,dm}$ can be obtained by multiplying this simulated result by $2\sqrt{2}$. For both circuits, the high noises at low frequencies were derived from the 1/f noise (or flicker noise) of each amplifier [21]. The modified TIA, despite its lower noise gain at low frequencies, presented a higher 1/f noise, which was probably caused by the 1/f noise contribution from the integrator circuit. Except for the 1/f noise region, the noise density curve of each circuit was generally consistent with each noise gain, as shown in Fig. 10(a). For the frequencies ranging from approximately 3 kHz to 3 MHz, the output noise of the modified TIA remained nearly constant at ~220 $\mathrm{nV}/\sqrt{\mathrm{Hz}}$ and was obviously dominated by the Johnson noise of R_{fT} that was ~200 $\mathrm{nV}/\sqrt{\mathrm{Hz}}$ (calculated from $(1+A)\sqrt{4kTR_{fT}}$). It then increased to 258 $\mathrm{nV}/\sqrt{\mathrm{Hz}}$ as a result of the noise gain peaking. In comparison, the output noise of the classic TIA remained nearly constant at ~60 $\mathrm{nV}/\sqrt{\mathrm{Hz}}$ in the frequency range from approximately 1 kHz to 500 kHz, where the dominant noise source was the Johnson noise of R_f that was ~57 $\mathrm{nV}/\sqrt{\mathrm{Hz}}$ (calculated from $\sqrt{4kTR_f}$). It then increased sharply to 328 $\mathrm{nV}/\sqrt{\mathrm{Hz}}$, exceeding the one in the modified TIA. That is, compared to a classic TIA, the modified TIA increased the feedback Johnson noise, which was the

Optics EXPRESS

dominant noise source at relatively lower frequencies, but greatly decreased the amplifier voltage noise, which was the dominant noise source at higher frequencies.

For the 300 m FOG application, the region of greatest interest lies within the desired signal bandwidth, from approximately 30 kHz to 3 MHz, in which the dominant noise source is the Johnson noise of $(1+A)\sqrt{4kTR_{fT}}$. To improve the SNR, which can be expressed as

$$\mathrm{SNR} = \frac{R_{feq}}{(1+A)\sqrt{4kTR_{fT}}} = \sqrt{\frac{R_{feq}}{4kT(1+A)}} = \sqrt{\frac{R_{fT}}{4kT}}, \tag{8}$$

it is desirable to minimize the amplifying factor (1 + A) (or maximize the value of R_{fT}), without sacrificing the bandwidth and gain performance. In our design, the amplifying factor (1 + A) is set to 11, which increases the noise within the signal bandwidth by approximately 3 times. However, as in any optical system, the theoretical sensitivity of the FOG is usually limited by the photon shot noise and coupled interference [1,26]. Therefore, the increased intrinsic noise has little effect on the FOG performance.

4. Experimental results

4.1 Circuit performance test

The modified circuit was assembled and tested in our 300 m FOG, using the same component values as in Section 3.2, as shown in Fig. 11. Note that the prototype circuit was not designed to be very compact, for the convenience of testing. The bandwidth was estimated by measuring the rise time of the circuit's output waveform, which is a simple and widely used method in high-speed applications [27]. As a rule of thumb, the relationship between the bandwidth f_{3db} (in GHz) and the rise time t_r (in ns) is $f_{3db} = 0.35/t_r$. The rise time, defined as the time from 10% of the final value to 90% of the final value, can be measured from the time-domain response of a square wave using an oscilloscope. As shown in Fig. 12, the measured rise time was 97.5 ns, implying a bandwidth of ~3.5 MHz. Although the actual bandwidth was less than half of the ideal bandwidth of ~8 MHz, as a result of the parasitic capacitance, it still met the design requirement.

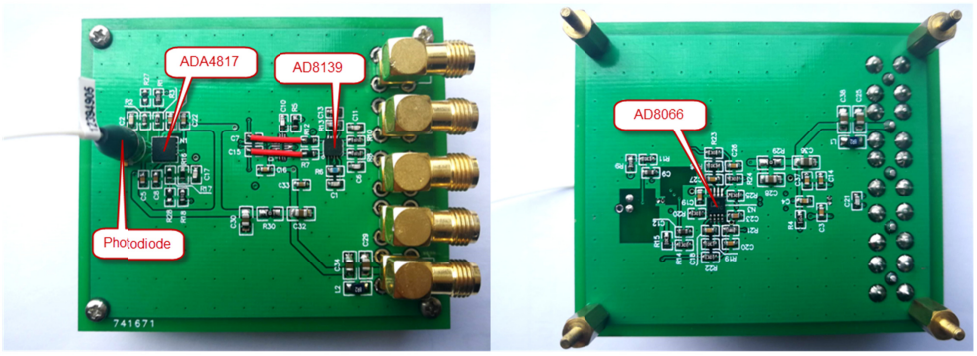

(a) (b)

Fig. 11. Photograph of the proposed fully differential photodiode amplifier: (a) front, (b) back.

Optics EXPRESS

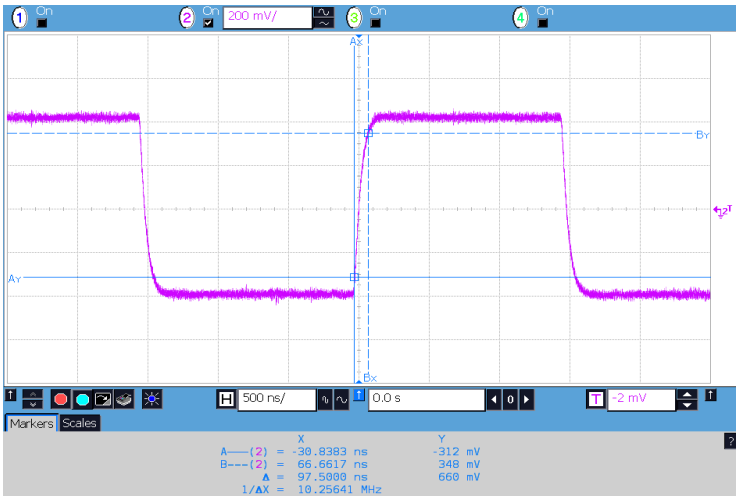

Fig. 12. Time-domain response of the modified circuit to a square wave with an amplitude of 800 mV. The rise time is 97.5 ns, indicating a bandwidth of ~3.5 MHz.

Measuring the circuit's inherent noise was somewhat complicated, because the noise spectrum was always dominated by extrinsic noises, such as, the power-line pickup, monitoring noise, and switching power supply noise. Therefore, the circuit's susceptibility to coupled interference was examined instead. A sinusoidal 10 mV signal at 300 kHz (near the modulation frequency of the FOG) was applied to both the terminals of the photodiode via two coupling capacitors of 10 pF, as illustrated in Fig. 3(b). The spectra of the single-ended output (at the port e_{OP} in Fig. 7) and differential output (at the port V_{OP} in Fig. 7) were measured using a spectrum analyzer and are compared in Fig. 13.

The differential output showed good common-mode rejection of the coupled input, with 19 dB improvement (from −17.36 to −36.20 dBm) on the suppression of the 300 kHz interference. In addition, all other spectral peaks, probably caused by external electromagnetic signals, and the noise floor were reduced by ~10 dBm. It is worth noting that the noise floor demonstrated a slightly positive slope within the 3 MHz bandwidth, confirming the noise gain peaking that was predicted in Fig. 10(b), and it was further enhanced by the two coupling capacitors.

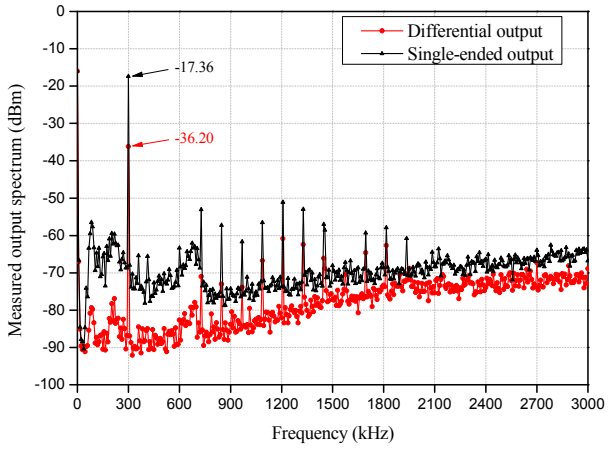

Fig. 13. Measured frequency spectra of the single-ended output port e_{OP} in Fig. 7 and the differential output port V_{OP} in Fig. 7.

Optics EXPRESS

4.2 FOG performance test

To verify this circuit's feasibility, the performance of the 300 m FOG using this circuit was tested, in terms of the ARW, bias drift, and dead band. For comparison, the performance of the same FOG using a PINFET receiver (rather than the classic TIA whose bandwidth is insufficient), with nearly the same signal gain and bandwidth as the differential circuit, was also tested.

The ARW defines the FOG's bias white noise and the bias drift represents the low-frequency variations of the FOG's output data. Both of them were evaluated by the Allan variance analysis of the FOG's stationary outputs. Figure 14 shows the Allan deviation of one-second bias data collected over five hours. The 300 m FOG using the differential circuit demonstrated an ARW of $0.014\,°/\sqrt{\text{h}}$ (or noise of $0.824\ (°/\text{h})/\sqrt{\text{Hz}}$), which was slightly better than the ARW of $0.015\,°/\sqrt{\text{h}}$ (or noise of $0.909\ (°/\text{h})/\sqrt{\text{Hz}}$) in the PINFET receiver case, and a bias drift of 0.03°/h, which was much better than the bias drift of 0.12°/h in the PINFET receiver case. It is reasonable to attribute this improvement in ARW and bias drift performance to the improved rejection of the coupled interference that has dominated the circuit's output noise. The significantly reduced bias drift can also be attributed to the greatly reduced low-frequency interference. A clearer demonstration of this performance improvement is shown in Fig. 15, where the bias data of five hours were averaged over 100 s to reduce the data variations to a level where the lower frequency bias-drift characteristics could be observed. There was a slow but large fluctuation in the bias data of the FOG using the PINFET receiver, leading to a large bias variation of 0.84°/h and hence a large bias drift. In comparison, there was no evidence of low-frequency data fluctuation in the differential circuit case, resulting in a reduced bias variation of 0.49°/h and hence a reduced bias drift.

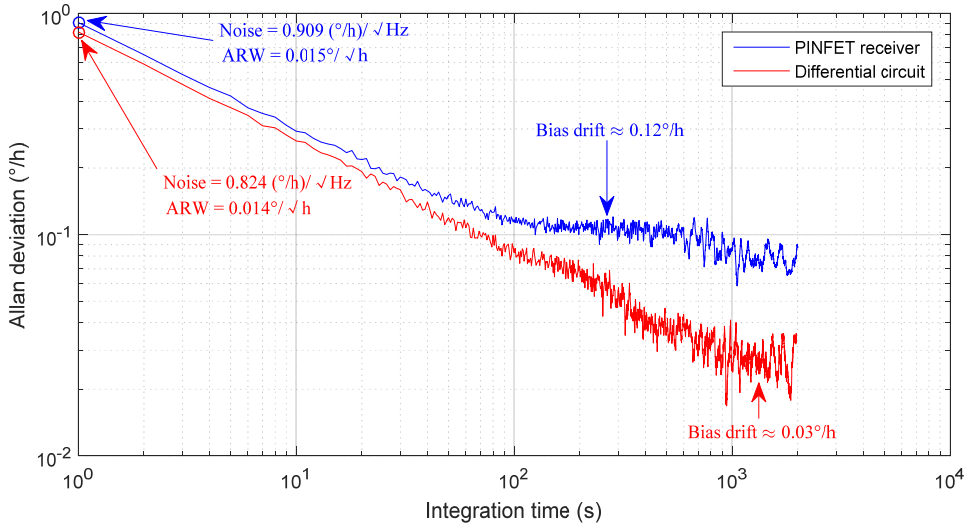

Fig. 14. Measured Allan deviation of a 300 m FOG using a PINFET receiver or the proposed fully differential photodiode amplifier.

Optics EXPRESS

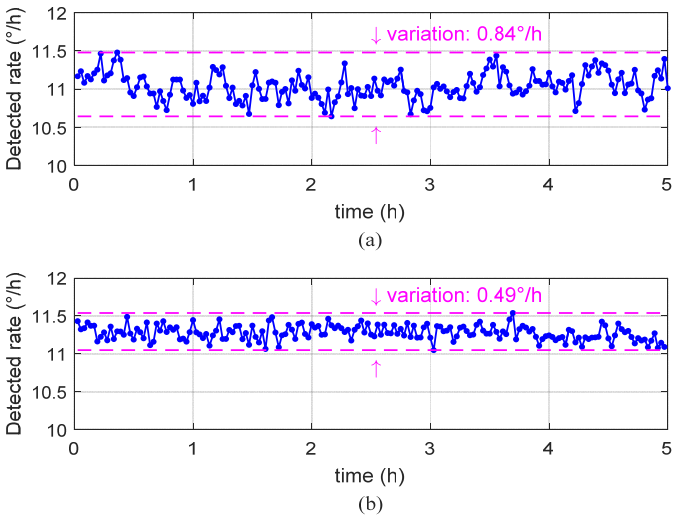

Fig. 15. Averaged bias data of the FOG using (a) the PINFET receiver or (b) the proposed fully differential photodiode amplifier.

A major concern related to the coupled interference is the dead band caused by the cross-coupling interference from the modulation voltage, which is examined in this section. The dead band was tested by mounting the FOG on a turntable with its sensitive axis pointing toward the east and rotating the turntable at a very low speed of 0.001°/s (corresponding to a rate step of 0.0002°/h for each second). Ultimately, the FOG scanned through a small fraction of the earth rate that ranged from approximately −2°/h to 2°/h. The measured data were averaged over 100 s to reduce the noise (resulting in the input rate resolution of 0.02°/h) and then plotted in terms of the input rate, as shown in Fig. 16. Even though the detected rate of the FOG using the PINFET receiver fluctuated widely around the ideal rate because of its poor noise performance, there was a distinct dead band of approximately 1.0°/h in the plot. In contrast, the differential circuit not only offered a more accurate detected rate, but also eliminated the dead band (or at least reduced it below the noise floor), proving its effective rejection of the cross-coupling interference.

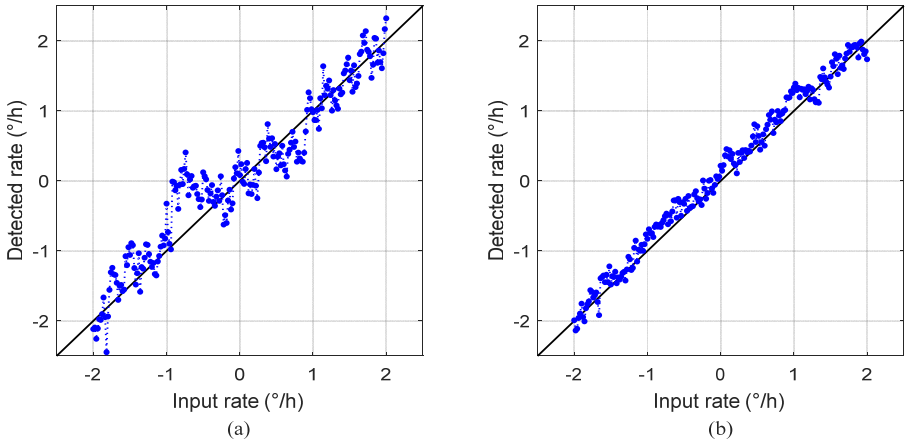

Fig. 16. Dead band measurement result of the FOG using (a) the PINFET receiver or (b) the proposed fully differential photodiode amplifier.

Optics EXPRESS

5. Conclusions

To suppress the effect of coupled interference in an FOG, we proposed a fully differential photodiode amplifier based on a three-op-amp instrumentation amplifier. Three major modifications were introduced to the instrumentation amplifier to improve its bandwidth: (1) a reverse bias was applied at two terminals of the photodiode to reduce the photodiode capacitance; (2) a tee-network was introduced to the feedback path to reduce the parasitic capacitance; and (3) a DC offset serve loop was introduced to eliminate the large DC offset caused by the bias voltage and tee-network. The intrinsic noise performance of the differential photodiode amplifier was analyzed and simulated, and it was observed that the tee-network reduced the SNR by a ratio of $\sqrt{1+A}$ within the bandwidth of interest, where A was the amplification ratio of the tee-network. However, it has little effect on the FOG performance because the output noise is dominated by the photon shot noise and coupled interference. In an experimental FOG with a 300 m fiber coil, we demonstrated the fully differential photodiode amplifier with a gain of 880 kΩ and bandwidth of 3.5 MHz. To the best of our knowledge, this is the first fully differential photodiode amplifier suited for FOGs, which provides not only the required wide bandwidth, high gain, and low noise but also good rejection of coupled interference. In the circuit performance test, the differential circuit exhibited 19 dB improvement in suppression of the applied common-mode interference, over the single-ended circuit, as well as improved noise performance. In the FOG performance test, the differential circuit not only improved the ARW from 0.015 to $0.014\,°/\sqrt{\mathrm{h}}$ and the bias drift from 0.12 to 0.03°/h (by greatly reducing the low-frequency interference) but also eliminated the approximately 1°/h dead band observed in the FOG using a PINFET receiver. These experimental results proved that using the proposed differential photodiode amplifier was an efficient solution for suppressing the coupled interference and an appealing way to improve the FOG performance.

In future work, compact design of the fully differential photodiode amplifier should be developed to improve the feasibility of miniature FOGs. Adding an electromagnetic shielding is beneficial for further improvement in the rejection of interfering signals. It is worth noting that the fully differential photodiode amplifier can be employed in other high-sensitivity photocurrent-sensing applications, such as, optical tomography and optical biosensor by properly adjusting the bandwidth and gain [12,13]. The method of using the modified tee-network and integrator circuit to eliminate the DC offset can be useful in other similar applications that need DC offset cancellation, such as, laser radar [26].

Funding

National Natural Science Foundation of China (NSFC) (61575012, 61575013).

Acknowledgments

We thank our colleagues Jingming Song, Wei Cai, and Zuchen Zhang for their technical help and language polishing, as well as Lei Wang for his participation in experiments.

References

1. H. C. Lefèvre, *The Fiber-Optic Gyroscope* (Artech House, 2014).
2. G. A. Sanders, S. J. Sanders, L. K. Strandjord, T. Qiu, J. Wu, M. Smiciklas, D. Mead, S. Mosor, A. Arrizon, W. Ho, and M. Salit, "Fiber optic gyro development at Honeywell," in *Fiber Optic Sensors and Applications XIII*, E. Udd, G. Pickrell, and H. H. Du, eds., Proc. SPIE **9852,** 985207 (2016).
3. I. R. Edu, R. Obreja, and T. L. Grigorie, "Current technologies and trends in the development of gyros used in navigation applications-a review," in Proceedings of the 5th WSEAS International Conference on Communications and Information Technology, (World Scientific and Engineering Academy and Society, 2011), pp. 63–68.
4. F. Dell'Olio, T. Tatoli, C. Ciminelli, and M. N. Armenise, "Recent advances in miniaturized optical gyroscopes," J. Eur. Opt. Soc. Rapid Publ. **9**, 14013 (2014).

Optics EXPRESS

5. C. Zhang, S. Zhang, X. Pan, and J. Jin, "Six-state phase modulation for reduced crosstalk in a fiber optic gyroscope," Opt. Express **26**(8), 10535–10549 (2018).
6. K.-H. Chong, W.-S. Choi, and K.-T. Chong, "Analysis of dead zone sources in a closed-loop fiber optic gyroscope," Appl. Opt. **55**(1), 165–170 (2016).
7. D. A. Egorov, R. O. Olekhnovich, A. A. Untilov, A. S. Aleinik, G. B. Deineka, and V. E. Strigalev, "Study on dead zones of fiber-optic gyros," Gyroscopy Navigation **2**(4), 197–207 (2011).
8. P. A. Ward, "Interferometric fiber optic gyroscope with off-frequency modulation signals," 7,817,284. U.S. Patent. 2010 Oct 19.
9. J. Jing, T. Hai-Ting, P. Xiong, and S. Ning-Fang, "Electrical crosstalk-coupling measurement and analysis for digital closed loop fibre optic gyro," Chin. Phys. B **19**(3), 030701 (2010).
10. J. G. Mark, D. A. Tazartes, and A. Cordova, "Method and apparatus for overcoming cross-coupling in a fiber optic gyroscope employing overmodulation," 5,682,241. U.S. Patent. 1997 Oct 28.
11. G. Spahlinger, "Fiber optic Sagnac interferometer with digital phase ramp resetting via correlation-free demodulator control," 5,123,741 A. U.S. Patent. 1992 Jun 23.
12. P. Wright, K. B. Ozanyan, S. J. Carey, and H. McCann, "Design of high-performance photodiode receivers for optical tomography," IEEE Sens. J. **5**(2), 281–288 (2005).
13. H. Song, Y. Park, H. Kim, and H. Ko, "Fully integrated biopotential acquisition analog front-end IC," Sensors (Basel) **15**(10), 25139–25156 (2015).
14. R. Yun and V. M. Joyner, "A monolithically integrated phase-sensitive optical sensor for frequency-domain NIR spectroscopy," IEEE Sens. J. **10**(7), 1234–1242 (2010).
15. D. A. Tazartes, J. E. Higbee, J. A. Tazartes, J. K. P. Flamm, and J. G. Mark, "Ultra low noise optical receiver," 5,521,555A. U.S. Patent. 1996 May 28.
16. R. A. Kovacs, "Fiber optic angular rate sensor including arrangement for reducing output signal distortion," 5,430,545A. U.S. Patent. 1995 Jul 4.
17. T. J. Bingel, D. E. Smith, S. J. Sanders, D. T. Vo, C. G. Ross, and D. Mead, "High-linearity signal-processing amplifier," 8,680,911. U.S. Patent. 2014 Mar 25.
18. J. Nayak, "Fiber-optic gyroscopes: from design to production," Appl. Opt. **50**(25), E152–E161 (2011).
19. H. Medjadba, S. Lecler, L. M. Simohamed, A. Chakari, and N. Javahiraly, "Optimizing the optical components choice for performances improvement of multimode fiber gyroscope," in *Photonics in the Transportation Industry: Auto to Aerospace II*, A. A. Kazemi, B. C. Kress, eds., Proc. SPIE **7314,** 731408 (2009).
20. M. Massarotto, A. Carlosena, and A. J. Lopez-Martin, "Two-stage differential charge and transresistance amplifiers," IEEE Trans. Instrum. Meas. **57**(2), 309–320 (2008).
21. J. G. Graeme, *Photodiode Amplifiers: Op Amp Solutions* (McGraw-Hill, 1996).
22. W. G. Jung, *Op Amp Applications Handbook* (Newnes, 2005).
23. D. Li, G. Minoia, M. Repossi, D. Baldi, E. Temporiti, A. Mazzanti, and F. Svelto, "A low-noise design technique for high-speed CMOS optical receivers," IEEE J. Solid-State Circuits **49**(6), 1437–1447 (2014).
24. M. Johnson, *Photodetection and Measurement: Maximizing Performance in Optical Systems* (McGraw-Hill, 2003).
25. S. Franco, *Design with Operational Amplifiers and Analog Integrated Circuits* (McGraw-Hill, 2002).
26. D. Nordin and K. Hyypp, "Single-stage photodiode op-amp solution suited for a self-mixing FMCW system," IEEE Trans. Instrum. Meas. **52**(6), 1820–1824 (2003).
27. E. Bogatin, *Signal and Power Integrity—Simplified, Second Edition* (Prentice-Hall, 2010).